SCATTERING ANALYSIS FOR SHIP KELVIN WAKES ON TWO-DIMENSIONAL LINEAR AND NONLINEAR SEA SURFACES

Rong-Qing Sun[1], Min Zhang[1, *], Chao Wang[2], and Xiao-Feng Yuan[2]

[1]School of Science, Xidian University, Xi'an 710071, China

[2]Science and Technology on Electromagnetic Scattering Laboratory, Beijing 100854, China

Abstract—The ship Kelvin-wake models on two-dimensional (2-D) linear and nonlinear sea surfaces are combined with the second-order small-slope approximation method (SSA-II) to comparatively study the corresponding electromagnetic (EM) scattering characteristics. The nonlinear sea-surface models include the Choppy Wave Model (CWM) and the second-order Creamer model (Creamer (2)). Considering the limitations of using the ideal plane EM wave incident upon a rough sea surface of the limited size, the modified tapered wave is utilized as the incident wave to derive the scattering waves. Due to the fact that the nonlinear effects of Creamer (2) surfaces is obviously stronger than those of CWM surfaces, the bistatic normalized radar cross section (NRCS) calculated from Creamer (2) surfaces is significantly greater than that of its linear and CWM surfaces for scattering angles departing from the specular direction, and the backscattering coefficients from Creamer (2) surfaces are also the greatest except within quasi-specular (near vertical incidence) region. Moreover, for the linear and nonlinear sea surfaces, the influences of different wind speeds and directions on scattering characteristics are also calculated and analyzed in detail. However, taking the ship Kelvin wakes into account, the corresponding scattering features are obviously distinct from those of the single linear and nonlinear sea surfaces. This helps to provide a basis to extract the related ship information through the scattering characteristics of ship Kelvin wakes. Also it shows that the small-slope approximation method is a very effective analysis method to deal with the EM scattering from the rough sea surface.

1. INTRODUCTION

In recent decades, the study of the microwave scattering from oceanic surfaces has attracted a lot of attention. Ocean microwave remote sensing is of great significance in some aspects such as oceanic surveillance, target detection, wind speed inversion, ship parameters inversion through the wake system with the help of synthetic aperture radar (SAR) [1–5], etc. For spaceborne or airborne radar detection, the received power can be calculated by radar cross section of the radar equation [6–8]. For a sailing ship in the sea, an apparent wave zone will appear behind the ship with long continuous time and length up to several kilometers, which can be caused by the extension of the hull surface boundary layer, propeller disturbance, sea wave effect, etc. [9]. Since the wake has very distinctive characteristics and can last longer time than the ship itself, the wake's coverage is wider, and the detection probability is also much higher. With the development of SAR imaging and detection technology, the SAR can use the characterization of ship wake to detect and recognize the ship. The ship Kelvin wake is one of the most obvious ship wakes and easily identifiable, so the study of its EM scattering features is of great significance.

For the ship Kelvin wake, its oceanic background seriously affects its scattering characterization. The major sea backgrounds include linear and nonlinear surfaces. In general, linear sea surfaces are frequently used [10]. However, under some complex circumstances that the hydrodynamic nonlinearities of the sea waves should be considered, such as scattering analysis and Doppler spectral interpretation, the simplest linear sea models are not complete. In this paper, we give two kinds of nonlinear sea surfaces, i.e., CWM model and Creamer (2) model. For the CWM model, it is analytically tractable, numerically efficient, and robust to the inclusion of high frequencies and is based on horizontal rather than vertical local displacement of a linear surface [11]. For the Creamer (2) model, it is based on the Hamiltonian formalism under the weak wave-turbulence theory and is performed through the nonlinear transformation of the Hilbert transform of the linear surface [12, 13]. Finally, the linear superpositions of the ship Kelvin wakes on the linear and nonlinear sea surfaces provide the special geometric models for the scattering analysis.

As for the EM scattering theory from the rough surfaces, Bahar and Lee [14, 15] proposed the full wave method in early research mainly for the theory. In recent years, some relevant numerical methods appear, such as the extended boundary condition method (EBCM), Monte Carlo (MC) and the finite difference of the time-domain (FDTD) method. However, a widely popular approximate theory is

from the SSA method, which consists of a basic approximation of the theory (SSA-I) related to the elevation and second-order corrections to it (SSA-II) through the slope of the surface, and has been widely applied to evaluate microwave scattering from sea surfaces [16–19]. Additionally, the SSA method bridges the gap between the Kirchhoff approximation (KA) and the small perturbation method (SPM) [20–22]. Some scholars have applied the SSA method to the random sea surfaces with statistical significance [23]. Therefore, this paper adopts the SSA method to calculate and analyzes the scattering results from the ship Kelvin wakes on the linear, CWM and Creamer (2) sea surfaces.

In this paper, we focus on the markedly different features of the EM scattering from ship Kelvin wakes on the 2-D linear and nonlinear sea surfaces, which is realized by the SSA method. Based on these different scattering characteristics, it is very useful for ship parameter inversion and radar detection through the analysis on the obtained scattering results from ship Kelvin wakes on the sea surfaces of different kinds. Moreover, the impacts of the nonlinearity from sea surfaces on EM scattering features of ship Kelvin wakes are analyzed in detail, which further provides a basis to extract the related ship information from different sea backgrounds.

The remainder of this paper is organized as follows. In Section 2, we focus first on the linear surface that is the comparative reference to our nonlinear models. Then, we present the nonlinear models based on the CWM and Creamer (2) model and the required computation cost. Additionally, in Section 3, the ship Kelvin wake models are also presented in detail. In Section 4, the tapered incident wave is introduced, and the EM scattering calculations are performed by utilizing SSA-II is presented. Section 5 is devoted to results and comments. This paper ends with concluding section and acknowledgements.

2. 2-D LINEAR AND NONLINEAR SEA-SURFACE REALIZATION

2.1. Linear Sea Surface Model

As for fully developed deep-water sea, the linear surface can be realized by the spectral method under the spatially homogeneous and time-stationary hypothesis, which is supposed to be a superposition of harmonics whose amplitudes are independent Gaussian random variables with variances proportional to a certain wind-dependent sea spectrum. Then each harmonic wave is allowed to propagate

independently of other waves according to the water-wave dispersion relation, which can define the sea surface profile at any later time.

The linear sea surface can be generated by Fourier transform of the sea spectrum. The spatial Fourier components at any time t can be written as [13]

$$A\left(\vec{k},t\right) = \gamma\left(\vec{k}\right)\sqrt{2P\left(\vec{k}\right)\delta k_x \delta k_y}e^{-i\omega t} \qquad (1)$$

where γ is a complex Gaussian process with zero mean and unity standard deviation. $\vec{k}$ is the spatial wavenumber vector, which is equivalent to (k_x, k_y) and (k, φ). $P(\vec{k})$ is the sea spectrum, which is chosen as Pierson-Moskowitz (PM) [24]. For gravity waves, ω satisfies the dispersion relation $\omega^2 = gk$ and g is the gravity acceleration constant. The discretization step $\delta k_x = 2\pi/L_x$ and $\delta k_y = 2\pi/L_y$ are thus related to the lengths L_x and L_y of the surface in the x- and y-directions, respectively.

The discretized form of the sea surface elevation can be expressed as

$$h\left(\vec{r},t\right) = \mathrm{Re}\sum_{k} A\left(\vec{k},t\right)\exp\left(i\vec{k}\cdot\vec{r}\right) \qquad (2)$$

The sum (2) can be efficiently performed by inverse fast Fourier transform (IFFT):

$$h\left(\vec{r},t\right) = \mathrm{Re}\left[\mathcal{F}^I\left(A\left(\vec{k},t\right)\right)\right] \qquad (3)$$

The generation of one linear surface with N sampling points involves a number of floating-point operations of order $N\log N$.

2.2. CWM Sea Surface Model

The nonlinear hydrodynamic model CWM is based on a Lagrangian description of sea wave motion, and can be generated by horizontal displacement of Hilbert transform of an aforementioned linear surface. The displacement is expressed as

$$\vec{C}\left(\vec{r},t\right) = \sum_{\vec{k}} -i\frac{\vec{k}}{k}h(\vec{r},t)\exp\left(i\vec{k}\cdot\vec{r}\right) \qquad (4)$$

Utilizing this vector field, the horizontal position of a grid point of the sea surface is now $\tilde{\mathbf{r}} = \vec{r} + \vec{C}(\vec{r},t)$, with elevation $\tilde{h}(\tilde{\mathbf{r}},t) = h(\vec{r},t)$ which belongs to the linear sea surface.

Similar to the expression (2), the sum (4) can also be efficiently calculated through IFFT. And one CWM surface with N sampling points involves a number of floating-point operations of order $N\log N$.

2.3. Creamer (2) Sea Surface Model

The Creamer formulation writes as a nonlinear transformation of the
Hilbert transform of the linear sea surface. In the 2-D case, this Hilbert
transform is defined as a vector. At a given time t, its expression, which
is derived from (2), is

$$\vec{h}_t\left(\vec{r}\right) = \mathrm{Re}\sum_{\vec{k}} \left(-i\frac{\vec{k}}{k}\right) A\left(\vec{k}, t\right) \exp\left(i\vec{k}\cdot\vec{r}\right) \tag{5}$$

The Hilbert transform can be computed by IFFT, at the cost of
$N \log N$. The Creamer nonlinear transform is written as

$$C_t\left(\vec{k}\right) = \frac{1}{N}\sum_{\vec{r}} \frac{\exp\left[i\vec{k}\cdot\vec{h}_t\left(\vec{r}\right)\right] - 1}{k} \exp\left(-i\vec{k}\cdot\vec{r}\right) \tag{6}$$

However, this transform can not be performed by IFFT, because
the term $\exp[i\vec{k}\cdot\vec{h}_t\left(\vec{r}\right)]$ depends on both $\vec{k}$ and $\vec{r}$. Moreover, the
Creamer method reveals to have also a N^2 numerical cost. In order to
solve the problem, we expand the exponential operator as a series, i.e.,
$C_t = \sum_{n\geq 1} C_t^n$, with

$$C_t^n\left(\vec{k}\right) = \frac{1}{N}\sum_{\vec{r}} \frac{\left[i\vec{k}\cdot h_t\left(\vec{r}\right)\right]^n}{n!k} \exp\left(-i\vec{k}\cdot\vec{r}\right), \tag{7}$$

It is easy to verified that the first order of this series C_t^1 identifies
with $A(\vec{k}, t)$, which corresponds to the linear surface. Moreover, the
second-order term can be completely by FFT, i.e.,

$$C_t^2 = -\frac{k_x^2}{2k}\mathcal{F}\left[h_{tx}^2\right] - \frac{k_x k_y}{k}\mathcal{F}\left[h_{tx}h_{ty}\right] - \frac{k_y^2}{2k}\mathcal{F}\left[h_{ty}^2\right] \tag{8}$$

Finally, the Creamer (2) sea surface can be constructed by $h_t =
\mathrm{Re}\mathcal{F}^I[A + C_t^2]$.

2.4. Realizations of Linear and Nonlinear Sea Surface

The size of the sea surface is $25 \times 25\,\mathrm{m}$, and there are 512 sampling
points in x and y direction. The wind speed is $5\,\mathrm{m/s}$, and wind
direction is $45°$. The results are shown in Figures 1 and 2.

From the 2-D profiles, it is hard to see visually the differences
between the linear and CWM sea surfaces; however, the nonlinear
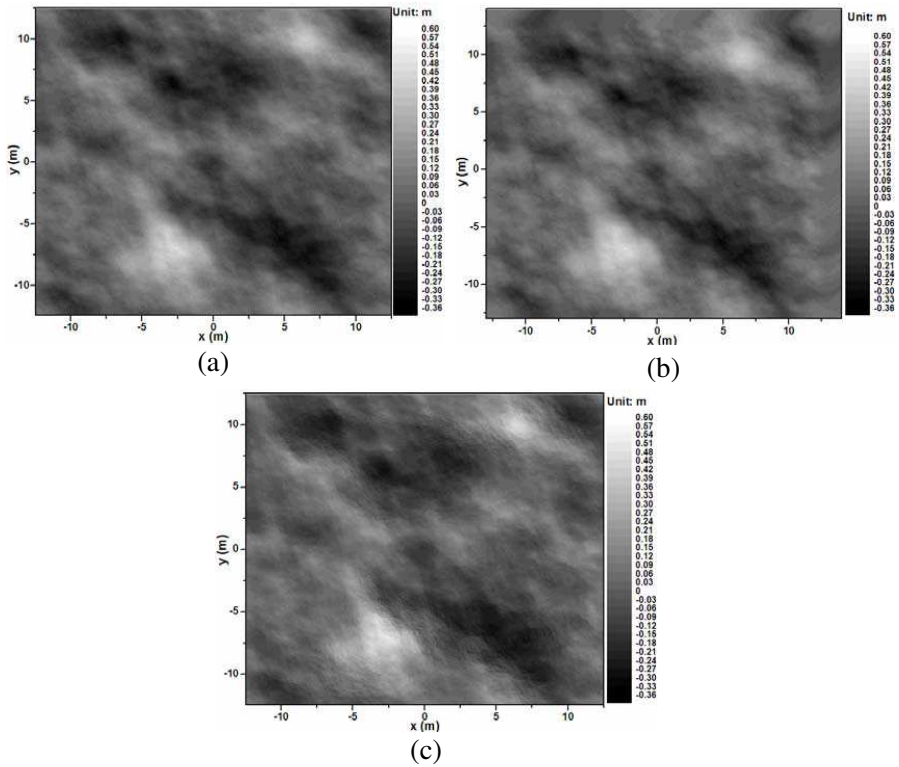characteristics of the Creamer (2) surfaces are obviously different from

(a)

(b)

(c)

Figure 1. 2-D linear, CWM and Creamer (2) sea surfaces. Wind speed is 5 m/s and wind direction is 45°. (a) Linear sea surface. (b) CWM sea surface. (c) Creamer (2) sea surface.

others. Therefore, we extract samples in a particular scan direction and obtain the 1-D linear, CWM and Creamer (2) sea surfaces, as shown in Figure 2. It is clear that the troughs of the linear-wave component fall below the more rounded troughs of the Creamer (2) wave, whereas the peaks of the Creamer (2) wave are steeper than the corresponding linear waves. However, as for the CWM wave, this phenomenon is relatively weak corresponding to the Creamer (2) wave, which is because the nonlinear features are revealed though the horizontal displacements so that the particular warping actually sharpens the wave peaks and broadens the wave valleys to a certain extent.
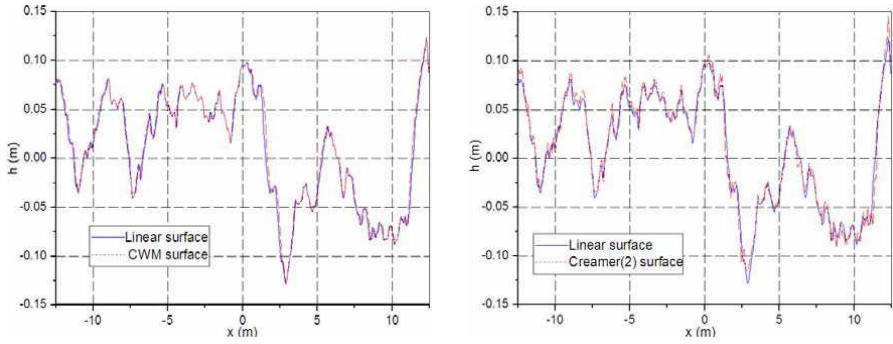
Figure 2. One-dimensional linear, CWM and Creamer (2) sea surfaces extracted from 2-D elevation profiles in Figure 1.

3. SHIP KELVIN WAKE

When the ship sails in the sea, an apparent wake zone will appear behind the ship with long continuous time and length up to several kilometers. Ship-wake systems mainly include Kelvin wake and turbulent wake which are two of the most important features in target identification on the oceanic background [25, 26]. The turbulent wake refers to the volume scattering of foam layers, and this paper only studies Kelvin wakes of ships.

Kelvin wakes contain two distinct waveforms: divergent waves and transverse waves. The largest surface area of wake is limited with the range between $16°$ and $19.5°$ on both ship sides. Additionally, the wave elevation distribution of Kelvin wakes has already had certain expressions beneficial to the study of all kinds of ships' sizes and velocities [28]. In this case, its expression can be written as

$$\eta(x, y) = \text{Re} \int_{-\pi/2}^{\pi/2} F(\theta) \cdot \exp\left[k \sec^2 \theta (ix \cos \theta + iy \sin \theta)\right] d\theta \quad (9)$$

where $k = g/U_s^2$, g is the acceleration of gravity, θ the angle between the wave direction and x axis, and $F(\theta)$ the free spectrum that describes the ship's features. Its expression is

$$F(\theta) = 4k \sec^3 \theta H \left(k \sec^2 \theta, \theta\right) / U_s \quad (10)$$

where $H(k, \theta)$ is Kochin function and can be written as

$$H(k, \theta) = \iint_{S_H} \sigma(x, y, z) \exp(k(ix \cos \theta + iy \sin \theta + z)) dS \quad (11)$$

where S_H is the ship's hull surface, and $\sigma(x, y, z)$ depicts the source strength, proportional to the local slope of the hull. Using the thin

ship approximation, the ship's hull is represented by a distribution of sources located on the longitudinal centreplane of the vessel. According to this theory, the source strengths are expressed as

$$\sigma(x, y, z) = -\frac{2V}{4\pi} \frac{\partial}{\partial x} f(x, z) \tag{12}$$

where f is the hull equation of the ship. A simple hull form (Wigley ship) is used to the wave elevation of the ship Kelvin wake, i.e.,

$$f(x, z) = \begin{cases} b & \left(1 - x^2/l^2\right)\left(-d < z < 0, -l < x < l\right) \\ 0 & (z < -d) \end{cases} \tag{13}$$

where b is the half-beam, l the half-length of the ship, and d the wall-sided draft.

In this paper, the size of the Kelvin wake is the same as the sea surface mentioned above. Given a ship, length $L = 52\,\text{m}$, beam $B = 5.7\,\text{m}$, draft $d = 3\,\text{m}$ and ship speed $U_s = 3\,\text{m/s}$. The results are shown in Figure 3 below. Figure 3(a) gives a single Kelvin wake, whereas Figure 3(b) shows the ship Kelvin wake on the linear sea surface with wind speed of $3\,\text{m/s}$ and wind direction of $45°$. It is pointed out that the direct superposition of the ship wake on the sea surface is performed. It is seen that from the figure, the effect of the sea background on the ship Kelvin wake is very significant. As we know, the ship wake will be drown into the sea when wind speed is far greater than ship speed.
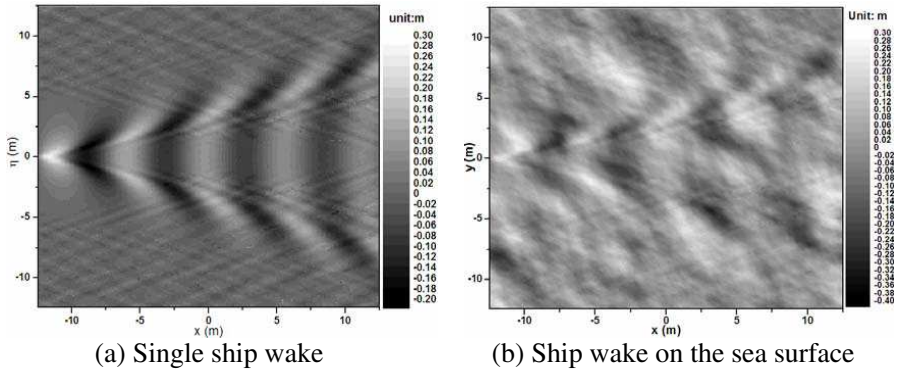

(a) Single ship wake   (b) Ship wake on the sea surface

Figure 3. The geometric model of the ship Kelvin wake. Ship speed is $3\,\text{m/s}$. (a) Single ship wake. (b) Ship wake on the sea surface with wind speed of $3\,\text{m/s}$ and wind direction of $45°$.

4. SCATTERING FIELD THEORY

The geometrical configuration adopted to solve the wave-scattering problem from the 2-D randomly-rough surface is given in Figure 4, where a rough interface $z = h(\vec{r})$, with $\vec{r} = (x, y)$, between two homogenous half-spaces, is considered [29–32]. The time dependence is assumed to be $\exp(-i\omega_e t)$. And $\boldsymbol{\theta}_i$ and $\boldsymbol{\theta}_s$ are, respectively, incident and scattering elevation angles, and ϕ_i and ϕ_s are the incident and scattering azimuth angles, respectively. The incident wave vector can be expressed as $\vec{\mathbf{K}}_{ei} = \vec{k}_{e0} - q_{e0}\hat{z}$, where $\vec{k}_{e0}$ and $-q_{e0}$ are horizontal and vertical projections of the incident wave vector, respectively. The scattered wave vector is $\vec{\mathbf{K}}_{es} = _e + q_e\hat{z}$, where $\vec{k}_e$ and q_e are appropriate components of the scattered wave vector, respectively. q_0 and q can be expressed as [33, 34]:

$$q_{e0} = \sqrt{\omega^2/c^2 - k_{e0}^2}, \quad q_e = \sqrt{\omega_e^2/c^2 - k_e^2}, \quad \mathrm{Im}q_{e0}, q_e \geq 0 \qquad (14)$$

In numerical simulations, the rough surface of the limited size forces the surface current to be zero for outside the rough surface. In this case, there is an abrupt change of surface current from nonzero to zero, which leads to the occurrence of artificial reflection from the boundaries. To circumvent these difficulties, one way is to taper the incident wave so that the incident wave gradually decays to zero in a Gaussian manner for the place closed to the boundaries [35–37].

In this paper, the tapered incident field can be expressed as:

$$\psi_{inc}\left(\vec{R}\right) = T\left(\vec{R}\right) q_{e0}^{-1/2} \exp\left(-i\vec{K}_{ei} \cdot \vec{R}\right) \qquad (15)$$
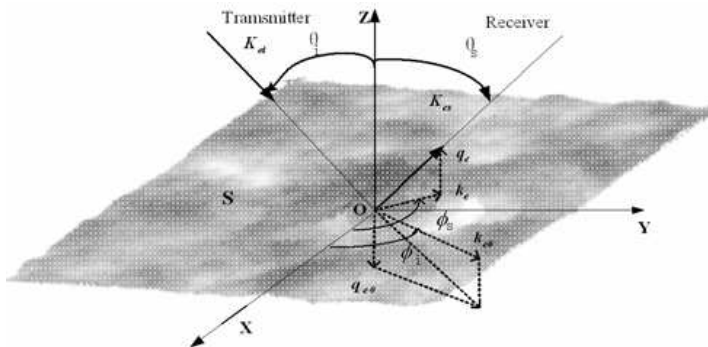

Figure 4. Geometry configuration for the wave scattering from 2-D surface.

$$T\left(\vec{R}\right) = \exp\left[-i\left(\vec{K}_{ei} \cdot \vec{R}\right)w\right]\exp\left(-t\right) \tag{16}$$

where $\vec{R} = \left(\vec{r}, h\right) = (x, y, z)$, $t = t_x + t_y$, and

$$t_x = (x\cos\theta_i\cos\phi_i + y\cos\theta_i\sin\phi_i + z\sin\theta_i)^2/(g^2\cos^2\theta_i) \tag{17}$$

$$t_y = (-x\sin\phi_i + y\cos\phi_i)^2/g^2 \tag{18}$$

$$w = \frac{1}{K_{ei}^2}\left(\frac{2t_x - 1}{g^2\cos^2\theta_i} + \frac{2t_y - 1}{g^2}\right) \tag{19}$$

ψ_{inc} is electric field E or magnetic field H depending on the polarization states and g the parameter that controls the tapering of the incident wave and directly affects the accuracy and validity of the scattering calculation.

The SSA-II method is chosen to deal with the scattering problem from the randomly rough dielectric surfaces, which has been revealed to be an effective model for rough surface scattering in several researches. After introducing the taper $T(\vec{R})$ into the integral term of the SSA-II method, the scattering amplitude can be revised as

$$\bar{\bar{S}}\left(\vec{k}_e, \vec{k}_{e0}\right)$$

$$= \frac{2(q_{e0}q_e)^{1/2}}{\sqrt{P_{inc}}(q_{e0} + q_e)}\int\frac{d\vec{r}}{(2\pi)^2}T\left(\vec{R}\right)\exp\left[-i\left(\vec{k}_e - \vec{k}_{e0}\right)\cdot\vec{r} + i(q_e + q_{e0})h\left(\vec{r}\right)\right]$$

$$\times\left[\bar{\bar{B}}\left(\vec{k}_e, \vec{k}_{e0}\right) - \frac{i}{4}\int\bar{\bar{M}}\left(\vec{k}_e, \vec{k}_{e0}; \vec{\xi}\right)h\left(\vec{\xi}\right)\exp\left(i\vec{\xi}\cdot\vec{r}\right)d\vec{\xi}\right] \tag{20}$$

where $\vec{r}$ is the projection component in the x-y plane of spatial location vector $\vec{R}$, and P_{inc} is the incident wave power received by the rough surface and can be expressed as:

$$P_{inc} = \iint|\psi_{inc}(x, y, 0)|^2 dxdy \tag{21}$$

$h(\vec{\xi})$ is the Fourier transform of $h(\vec{r})$, i.e.,

$$h\left(\vec{\xi}\right) = \int h\left(\vec{r}\right)\exp\left(-i\vec{\xi}\cdot\vec{r}\right)d\vec{r}/(2\pi)^2 \tag{22}$$

$\bar{\bar{B}}$, $\bar{\bar{B}}_2$ and $\bar{\bar{M}}$ are the 2×2 matrices describing mutual transformations of the EM waves of the different polarizations. The relation between them satisfies

$$\bar{\bar{M}}\left(\vec{k}_e, \vec{k}_{e0}; \vec{\xi}\right) = \bar{\bar{B}}_2\left(\vec{k}_e, \vec{k}_{e0}; \vec{k}_e - \vec{\xi}\right) + \bar{\bar{B}}_2\left(\vec{k}_e, \vec{k}_{e0}; \vec{k}_{e0} + \vec{\xi}\right)$$

$$+ 2(q_{e0} + q_e)\bar{\bar{B}}\left(\vec{k}_e, \vec{k}_{e0}\right) \tag{23}$$

where the corresponding matrix elements are B_{pq}, $B_{2,pq}$ and M_{pq}. Among them, subscripts "p" and "q" represent the vertical or horizontal polarizations. They are discussed in detail in [29, 34]. In addition, for the sake of convenience this paper only deals with co-polarizations HH and VV.

It is pointed out that this paper chooses medium 1 as air and medium 2 as dielectric sea surface. Therefore, the sea-surface dielectric constant is calculated using Debye formulas [38]. Moreover, the first-order small-slope approximation (SSA-I) can be generated if $\bar{\bar{M}} = 0$.

In terms of rough surface scattering amplitudes calculated by SSA-II, the NRCS from a rough sea surface can be obtained by

$$\sigma_{pq}^0 = 4\pi q q_0 \Delta S_{pq}\left(\vec{k}_e, \vec{k}_{e0}\right)\left(\Delta S_{pq}\left(\vec{k}_e, \vec{k}_{e0}\right)\right)^* \tag{24}$$

where subscript pq denotes polarization state, and

$$\Delta S_{pq}\left(\vec{k}_e, \vec{k}_{e0}\right) = S_{pq}\left(\vec{k}_e, \vec{k}_{e0}\right) - \left\langle S_{pq}\left(\vec{k}_e, \vec{k}_{e0}\right)\right\rangle \tag{25}$$

Due to the random features of the rough sea surface, the final bistatic NRCS and the backscattering coefficient are calculated as an average, i.e.,

$$\overline{\sigma_{pq}^0} = \left\langle \sigma_{pq}^0 \right\rangle \tag{26}$$

5. NUMERICAL RESULTS AND ANALYSIS

In the following simulations, we choose the SSA-II method to deal with the scattering problem. For the simulations of bistatic NRCS and backscattering coefficients, the sizes of all the surfaces are $L_x = L_y = 25$ m sampled with 512 points in each direction. The frequency is 1.2 GHz with the calculated relative dielectric constant $\varepsilon = (73.5, 61)$, tapering parameter g chosen to be $L_x/6$, and the averaged NRCS and backscattering coefficient are obtained over 100 realizations of the surfaces. In addition, as for a moving ship, its length is 52 m, beam is 5.7 m and draft is 3 m.

5.1. NRCS Comparisons of Linear with Nonlinear Sea Surfaces

The average bistatic NRCS results versus scattering angles from linear, CWM and Creamer (2) sea surfaces for indent angles of $0°$ and $60°$ in wind direction angle of $45°$ are shown in Figures 5(a), (b) (wind speed of 3 m/s). It is seen that the average NRCS values, from the largest to smallest, are Creamer (2), CWM and linear sea surfaces for the scattering angles departing from specular directions. For the
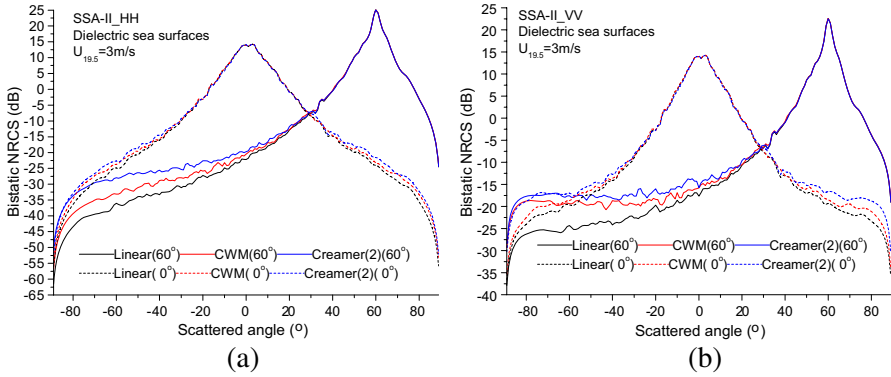
Figure 5. Average bistatic NRCS results versus scattering angles for incidence of 0° and 60° (a), (b) from linear, CWM and Creamer (2) sea surface. Wind speed is 3 m/s and direction is 45°.
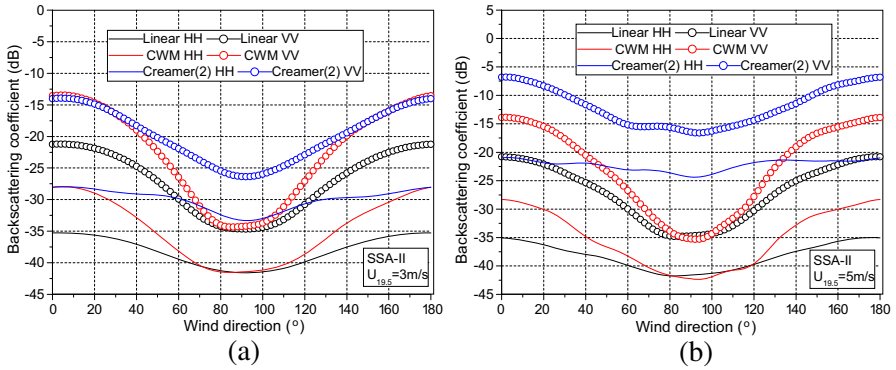

Figure 6. Backscattering coefficients versus wind-direction angles from linear, CWM and creamer (2) sea surfaces with wind speed of (a) 3 m/s and (b) 5 m/s for incident angle of 60°.

incidence of 60°, the differences just appear at negative scattering angles, whereas for the incidence of 0°, the distinctions exist for both backward and forward directions. However, near the specular direction, such distinctions for three surface models are minor.

The backscattering coefficients versus wind direction angles for the incidence of 60° are shown in Figure 6. It is seen that the minor discrepancies of backscattering coefficients between the linear and CWM surfaces exist in the crosswind direction (wind direction angle of 90°), while the corresponding largest differences lie in the downwind (wind direction angle of 180°) and upwind (wind direction angle of 0°)

directions. These differences are just contrary to those between the CWM and Creamer (2) surfaces. In addition, it is interesting to find that, in Figure 6(b), the backscattering coefficient for CWM surfaces is significantly higher than that of the linear surface for both upwind and downwind directions, while for those near the crosswind direction, we obtain the opposite observations.

5.2. Scattering Analysis of Ship Kelvin Wakes on Linear and Nonlinear Sea Surfaces

Figure 7 shows the scattering comparisons of the ship Kelvin wakes on the linear, CWM and Creamer (2) surfaces with the single-linear and nonlinear surface counterparts. Moreover, some parameters of sea surface and ship have been given above. Herein, for Figure 7, wind speed is $3\,\text{m/s}$, wind direction angle $45°$, and ship speed $3\,\text{m/s}$. Similarly, different from Figure 7, both the ship speed and wind speed are modified as $5\,\text{m/s}$ in Figure 8.

For average bistatic NRCS, from these figures, it is seen that, in the vicinity of specular direction, the average NRCS values from single linear and nonlinear sea surfaces are significantly larger than those of the corresponding surfaces with ship Kelvin wakes. And with the increase of ship speed, the average NRCS values of the linear and nonlinear surfaces with ship Kelvin wakes become much smaller. On the contrary, as the scattering angles gradually departing from the specular regions, the average NRCS from the surfaces with ship Kelvin wakes is evidently higher than that of single surface counterpart. In addition, it is interesting to find that, in Figures 8(a), (b), (c), (d), the specular ranges significantly moves towards the scattered angles which are less than the specular angles, because the higher roughness can arise from the Kelvin wave elevation when ship speed increases, which seriously affects the slope distribution of surface. In this case, the SSA-II method directly proportional to slope generates this kind of specular shift.

For the backscattering coefficients, from these figures, we can find that, in the quasi-specular region, the backscattering coefficients of single linear and nonlinear sea surfaces are evidently larger than those of the corresponding surface counterparts with ship Kelvin wakes. However, as the incident angle increases, the coefficients for the surfaces with ship Kelvin wakes are higher than those of single surface counterparts. And this phenomenon becomes more obvious when ship speed increases.
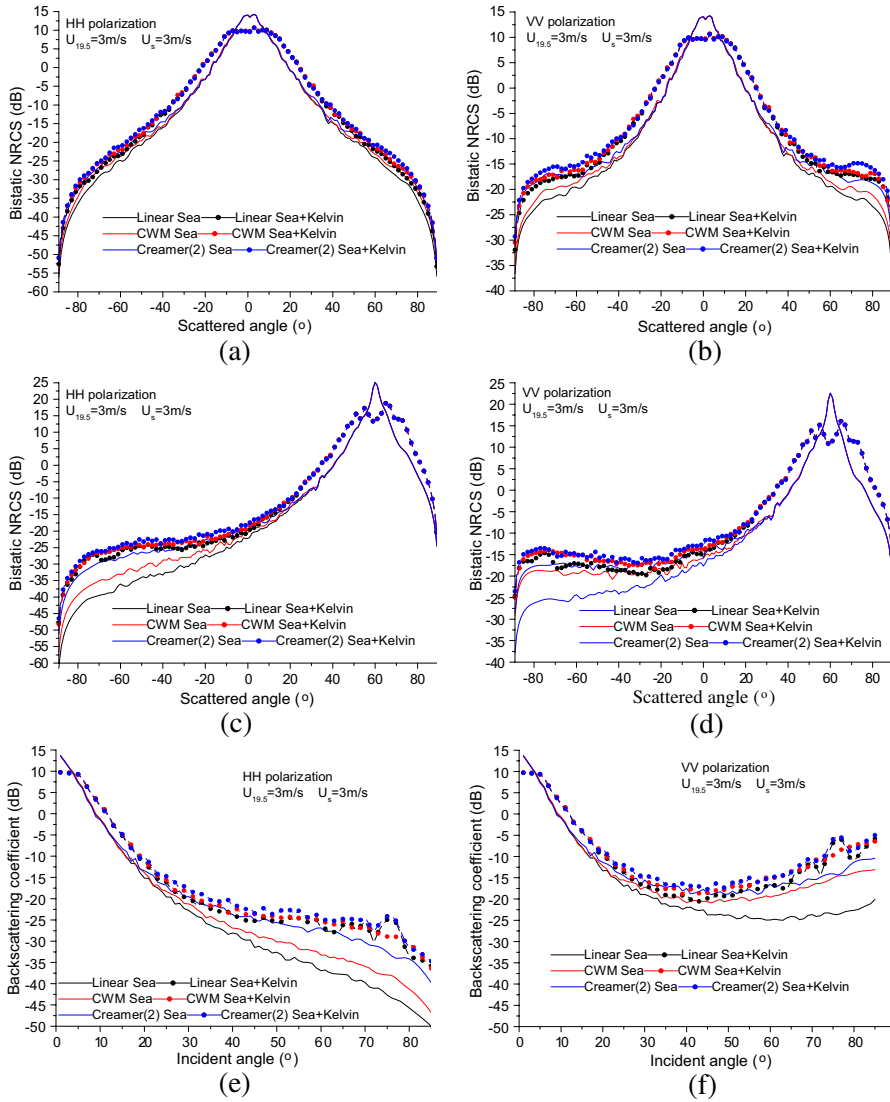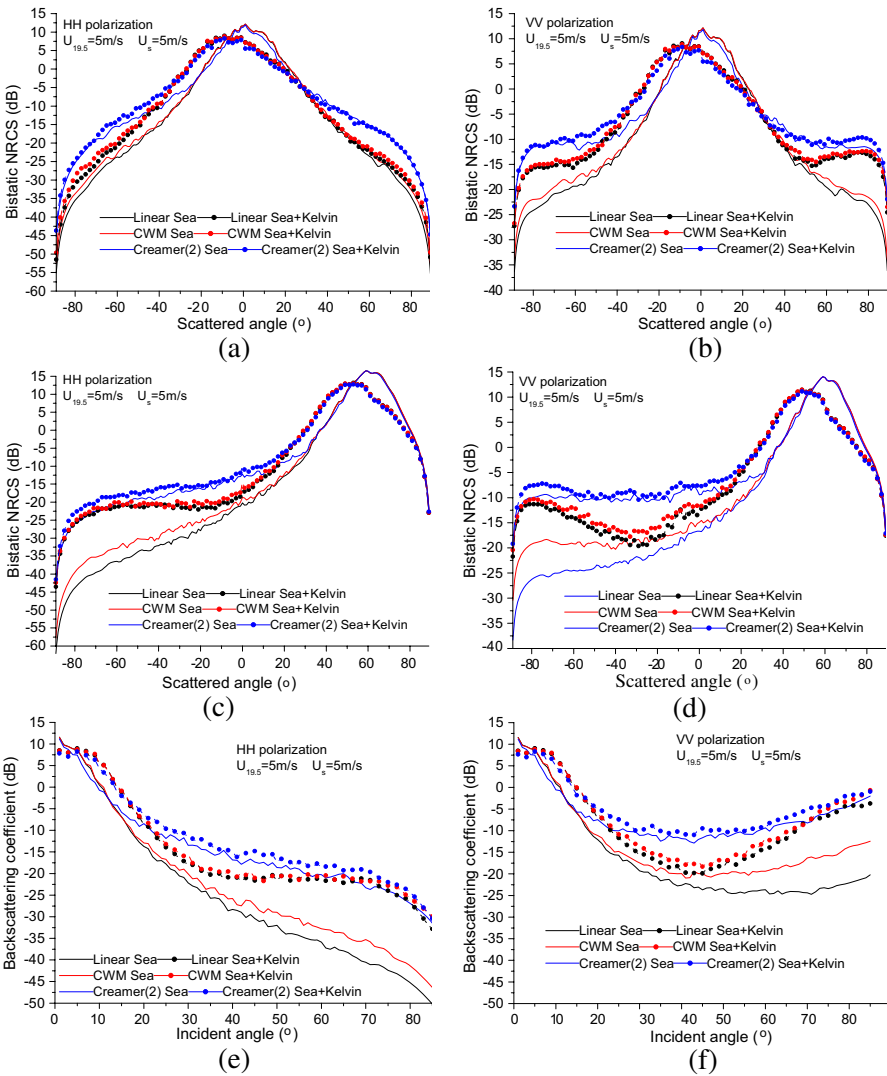
Figure 7. Scattering comparisons of the ship Kelvin wakes on the linear, CWM and Creamer (2) surfaces with the single linear and nonlinear surface counterparts, average bistatic NRCS for incident angles of $0°$ and $60°$ is shown in (a), (b), (c), (d) and backscattering coefficients versus incident angles are given in (e), (f). Wind speed is $3\,\text{m/s}$ and direction is $45°$. Ship speed is $3\,\text{m/s}$.

Figure 8. Scattering comparisons of the ship Kelvin wakes on the linear, CWM and Creamer (2) surfaces with the single linear and nonlinear surface counterparts, different from Figure 7, both the wind and ship velocities are 5 m/s.

6. CONCLUSION

In this paper, based on 2-D linear, CWM and Creamer (2) sea surfaces and ship Kelvin wakes, the SSA-II method has been utilized to calculate the corresponding scattering. A comparative study has been made to the features of NRCS and backscattering coefficients due to the hydrodynamic effects of ship Kelvin wakes. In addition, from the numerical results of bistatic NRCS and the backscattering coefficient, it is seen that the scattering signals from Creamer (2) sea surfaces are the strongest in three sea surfaces, whereas the backscattering coefficients of the CWM surfaces sometimes are less than those of the linear surfaces in the crosswind region. Moreover, considering the ship Kelvin wakes, the scattering effects of ship Kelvin wakes on the linear, CWM and Creamer (2) sea surfaces are significantly distinct, which is helpful for establishing better understanding of the scattering features of the ship Kelvin wakes on the linear and nonlinear sea surfaces and provide a basis on the extraction of ship-parameter information from the scattering characteristics of the ship Kelvin wakes.

REFERENCES

1. Zhao, Y. W., M. Zhang, X. Geng, and P. Zhou, "A comprehensive facet model for bistatic SAR imagery of dynamic ocean scene," *Progress In Electromagnetics Research*, Vol. 123, 427–445, 2012.

2. Ai, J., X. Qi, W. Yu, et al., "A novel ship wake CFAR detection algorithm based on SCR enhancement and normalized hough transform," *IEEE Trans. on Geosci. Remote Sens.*, Vol. 8, No. 4, 681–685, 2011.

3. Park, J.-I. and K.-T. Kim, "A comparative study on ISAR imaging algorithms for radar target identification," *Progress In Electromagnetics Research*, Vol. 108, 155–175, 2010.

4. Baussard, A. M., M. Rochdi, and A. Khenchaf, "PO/MEC-based scattering model for complex objects on a sea surface," *Progress In Electromagnetics Research*, Vol. 111, 229–251, 2011.

5. Nie, D. and M. Zhang, "Bistatic scattering analysis for two-dimensional rough sea surfaces using an angular composite model," *Int. J. Remote Sens.*, Vol. 32, No. 24, 9661–9672, 2011.

6. Bourlier, C. and G. Gerginc, "Microwave analytical backscattering models from randomly rough anisotropic sea surface — Comparison with experimental data in C and Ku bands," *Progress In Electromagnetics Research*, Vol. 37, 31–78, 2002.

7. Valenzuela, G. R., "Theories for the interaction of electromagnetic and oceanic waves — A review," *Boundary-layer Meteorology*," Vol. 13, 61–85, 1978.

8. Jin, Y. Q., "Numerical simulation of radar surveillance for the ship target and oceanic clutters in two-dimensional model," *Radio Science*, Vol. 38, No. 3, 1045, 2003.

9. Reed, A. M. and J. H. Milgram, "Ship wakes and their radar images," *Annu. Rev. Fluid Mech.*, Vol. 34, 469–502, 2002.

10. Sun, R.-Q., M. Zhang, C. Wang, and Y. Chen, "Study of electromagnetic scattering from ship wakes on PEC sea surfaces by the small-slope approximation theory," *Progress In Electromagnetics Research*, Vol. 129, 387–404, 2012.

11. Nouguier, F. C., et al., "Scattering from nonlinear gravity waves: The 'choppy wave' model," *IEEE Trans. on Geosci. Remote Sens.*, Vol. 48, No. 12, 4184–4192, 2010.

12. Creamer, D. B., F. Henyey, R. Schult, and J. Wright, "Improved linear representation of sea surface waves," *J. Fluid Mech.*, Vol. 205, 135–161, 1989.

13. Soriano, G., M. Joelson, and M. Saillard, "Doppler spectra from a two dimensional ocean surface at L-band," *IEEE Trans. on Geosci. Remote Sens.*, Vol. 44, No. 9, 2430–2437, 2006.

14. Bahar, E. and B. S. Lee, "Full wave solutions for rough-surface bistatic radar cross sections: Comparison with small perturbation," *Physical Optics, Numerical and Experimental Results. Radio Science*, Vol. 29, No. 2, 407–429, 1994.

15. Bahar, E. and B. S. Lee, "Radar scatter cross section for two-dimensional random rough surfaces-full wave solutions and comparisons with experiments," *Wave in Random Media*, Vol. 6, 1–23, 1996.

16. Vaitilingom, L. and A. Khenchaf, "Radar cross sections of sea and ground clutter estimated by two scale model and small slope approximation in hf-VHF bands," *Progress In Electromagnetics Research B*, Vol. 29, 311–338, 2011.

17. Voronovich, A. G., "Small-slope approximation in wave scattering

by rough surfaces," *Sov. Phys — JETP.*, Vol. 62, 65–70, 1985.

18. Berginc, G. and C. Bourrely, "The small-slope approximation method applied to a three-dimensional slab with rough boundaries," *Progress In Electromagnetics Research*, Vol. 73, 131–211, 2007.

19. Toporkov, J. V., et al., "Numerical study of the extended Kirchhoff approach and the lowest order small slope approximation for scattering from ocean-like surfaces: Doppler analysis," *IEEE Trans. on Antennas and Propagat.*, Vol. 50, No. 4, 417–425, 2002.

20. Chen, H., M. Zhang, and H.-C. Yin, "Faced-based treatment on microwave bistatic scattering of three-dimensional sea surface with electrically large ship," *Progress In Electromagnetics Research*, Vol. 123, 385–405, 2012.

21. Thorsos, E. I., "The validity of the Kirchhoff approximation for rough surface scattering using a Gaussian roughness spectrum," *J. Acoust. Soc. Am.*, Vol. 83, No. 1, 78–92, 1988.

22. Guo. L.-X., Y. Liang, J. Li, and Z.-S. Wu, "A high order intergral SPM for the conducting rough surface scattering with the tapered wave incidence — TE case," *Progress In Electromagnetics Research*, Vol. 114, 333–352, 2011.

23. Chevalier, B. and G. Berginc, "Small-slope approximation method: scattering of a vector wave from 2D dielectric and metallic surfaces with Gaussian and non-Gaussian statistics," *Proceedings of SPIE*, Vol. 4100, 22–32, 2000.

24. Fung, A. K. and K. K. Lee, "A semi-empirical sea-spectrum model for scattering coefficient estimation," *IEEE Journal of Oceanic Engineering*, Vol. 7, 166–176, 1982.

25. Shakeri, M., M. Tavakolinejad, and J. H. Duncan, "An experimental investigation of divergent bow waves simulated by a two-dimensional plus temporal wave marker technique," *J. Fluid Mech.*, Vol. 634, 217–243, 2009.

26. Hennings, R. R., W. Alpers, and A. Viola, "Radar imaging of Kelvin arms of ship wakes," *Int. J. Remote Sensing*, Vol. 20, No. 13, 2519–2543, 1999.

27. Milgram, J. H., R. A. Skop, R. D. Pelter, and O. M. Griffin, "Modeling short sea wave energy distributions in the far wakes of ships," *J. Geophys. Res.*, Vol. 98, No. C4, 7115–7124. 1993.

28. Sun, R. Q., G. Luo, M. Zhang, and C. Wang, "Electromagnetic scattering model of the Kelvin wake and turbulent wake by a moving ship," *Waves in Random Media*, Vol. 21, No. 3, 501–504, 2011.

29. Mcdaniel, S. T., "An extension of the small-slope approximation for rough surface scattering," *Waves in Random Media*, Vol. 5, No. 2, 201–214, 1995.

30. Luo, G. and M. Zhang, "Investigation on the scattering from one-dimensional nonlinear fractal sea surface by second-order small-slope approximation," *Progress In Electromagnetics Research*, Vol. 133, 425–411, 2013.

31. Albert, M. D., Y. J. Lee, H.-T. Ewe, and H.-T. Chuah, "Multilayer model formulation and analysis of radar backscattering from sea ice," *Progress In Electromagnetics Research*, Vol. 128, 267–290, 2012.

32. Voronovich, A. G. and V. U. Zavorotny, "Theoretical model for scattering of radar signals in Ku- and C-bands from a rough sea surface with breaking waves," *Waves in Random Media*, Vol. 11, No. 3, 247–269, 2001.

33. Zhang, M., W. Luo, G. Luo, C. Wang, and H.-C. Yin, "Composite scattering of ship on sea surface with breaking waves," *Progress In Electromagnetics Research*, Vol. 123, 263–277, 2012.

34. Voronovich, A. G., "Small-slope approximation for electromagnetic wave scattering at a rough interface of two dielectric half-spaces," *Waves in Random Media*, Vol. 4, 337–367, 1994.

35. Li, X. F. and X. J. Xu, "Scattering and doppler spectral analysis for two-dimensional linear and nonlinear sea surfaces," *IEEE Trans. on Geosci. Remote Sens.*, Vol. 49, No. 2, 603–611, 2011.

36. Berginc, G., "Small-slope approximation method: A further study of vector wave scattering from two-dimensional surfaces and comparison with experimental data," *Progress In Electromagnetics Research*, Vol. 37, 251–287, 2002.

37. Ji, W.-J. and C.-M. Tong, "Bistatic scattering from two-dimensional dielectric ocean rough surface with a PEC object partially embedded by using the G-SMCG method," *Progress In Electromagnetics Research*, Vol. 105, 119–139, 2010.

38. Stogryn A., "Equations for calculating the dielectric constant of saline water," *IEEE Trans. on Microw. Theory and Tech.*, Vol. 19, No. 8, 733–736, 1971.